Optical design for a see-through head-mounted display with high visibility

Kai-Wei Zhao[1] and Jui-Wen Pan[2,3,*]

[1]*Institute of Lighting and Energy Photonics, National Chiao Tung University, Tainan City 71150, Taiwan*
[2]*Institute of Photonic System, National Chiao Tung University, Tainan City 71150, Taiwan*
[3]*Department of Medical Research, Chi Mei Medical Center, Tainan City 71004, Taiwan*
[*]*juiwenpan@gmail.com*

Abstract: An optical design for a see-through head-mounted display with high visibility is described. This design, which is based on a light guide plate with triangular microstructures, can overcome the limitations of the balance in optical efficiency. The optical efficiency of the virtual image can be larger than the optical efficiency of the real image, which ensures high visibility. The visibility can be increased to 22 with this design, much higher than the visibility possible with previous designs for a see-through head-mounted display, making this suitable for daily application.

OCIS codes: (120.2820) Heads-up displays; (220.0220) Optical design and fabrication; (220.2740) Geometric optical design.

References and links

1. J. Rolland and O. Cakmakci, "Head-Worn Displays: The Future Through New Eyes," Opt. Photonics News **20**(4), 20 (2009).
2. H. Hua and B. Javidi, "Augmented Reality: Easy on the Eyes," Opt. Photonics News **26**(2), 26 (2015).
3. R. Azuma, Y. Baillot, R. Behringer, S. Feiner, S. Julier, and B. Macintyre, "Recent advances in augmented reality," IEEE Comput. Graph. Appl. **21**(6), 34–47 (2001).
4. Smart glasses, website *http://www.epson.com/cgi-bin/Store/jsp/Landing/moverio-bt-200-smart-glasses.do?ref=van_moverio_2014*.
5. B. Kress and T. Starner, "A review of head-mounted displays (HMD) technologies and applications for consumer electronics," Proc. SPIE **8720**, 87200A (2013).
6. J. Chen, W. Cranton, and M. Fihn, "Optical Components for Head-Worn Displays" in *Handbook of Visual Display Technology, Vol. 4* (Springer, 2012) pp. 2184.
7. J. P. Rolland and H. Hua, " Head-mounted display systems," *Encyclopedia of Optical Engineering*, R. G. Driggers, ed. (Taylor & Francis, 2003).
8. D. Cheng, Y. Wang, H. Hua, and M. M. Talha, "Design of an optical see-through head-mounted display with a low f-number and large field of view using a freeform prism," Appl. Opt. **48**(14), 2655–2668 (2009).
9. Z. Zheng, X. Liu, H. Li, and L. Xu, "Design and fabrication of an off-axis see-through head-mounted display with an x-y polynomial surface," Appl. Opt. **49**(19), 3661–3668 (2010).
10. Y.Amitai, "Extremely compact high-performance HMDs based on substrate-guided optical element," SID 2004 Digest **35**, 310–313 (2004).
11. Y. Amitai, "A two-dimensional aperture expander for ultra-compact, high-performance head-worn displays," SID 2005 Digest **36**, 360–363 (2005).
12. J. W. Pan and H. C. Hung, "Optical design of a compact see-through head-mounted display with light guide plate," J. Disp. Technol. **11**(3), 223–228 (2015).
13. G. Rajeswaran, M. Iton, M. Boroson, S. Barry, T. K. Hatwar, K. B. Kahen, K. Yoneda, R. Yokoyama, T. Yamada, N. Komiya, H. Kanno, and H. Takahashi, "Active metric low temperature poly-Si TFT/OLED full color displays: development status," SID Digest **31**, 974–977 (2000).
14. J. Warren, *Modern Optical Engineering* (McGraw Hill, 2008), pp. 128–129.
15. O. Cakmakci and J. Rolland, "Head-worn display: review," J. Disp. Technol. **2**(3), 199–216 (2006).
16. J. Chen, W. Cranton, and M. Fihn, "Example of HWD Architectures: Low-, Mid- and Wide- Field of View Designs," *Handbook of Visual Display Technology, Vol. 4* Springer, 2012) p. 2201.
17. J. Chen, W. Cranton, and M. Fihn, "Optical Components for Head-Worn Displays" *Handbook of Visual Display Technology, Vol. 4* (Springer, 2012) p. 2184.
18. J. Warren Smith, *Modern Optical Engineering* (McGraw Hill, 2008), pp.272.
19. E. Robert Fischer, B. Tadic-Galeb and P. R. Yoder, *Optical System Design* (McGraw Hill, 2008).
20. J. W. Pan, C. M. Wang, H. C. Lan, W. S. Sun, and J. Y. Chang, "Homogenized LED-illumination using microlens arrays for a pocket-sized projector," Opt. Express **15**(17), 10483–10491 (2007).

#257414 Received 28 Jan 2016; revised 18 Feb 2016; accepted 19 Feb 2016; published 25 Feb 2016

1. Introduction

In the past few years, head-mounted displays (HMDs) have undergone rapid development [1]. Recently, with the widespread availability of wireless networks, HMDs have become more popular for use in daily life and are now widely applied in a lot of fields for military, entertainment and medical applications [2]. HMDs can be classified as see-through or immersive. Immersive HMD systems only allow users to see virtual images, blocking out the real world scene (real images). See-through HMD systems have the capability of superimposing the virtual image on the real world scene and allow the users see the virtual image of the digital information and real world scene simultaneously [3]. For some applications, the see-through function plays an important role. For example, in military aircraft, the basic navigation and flight information can be superimposed on the user's view of the real world scene by the see-through function.These virtual images of digital information help the pilots to aim at and attack the target more accurately. See-through HMDs provide a new way for the user to obtain digital image information. Nowadays, some products have entered the market, such as smart glasses by EPSON [4] which shows that wearable devices with see-through HMDs have commercial potential.

Although many researchers have worked hard to make the see-through HMD devices both compact and lightweight [5], the design of a compact see-through HMD is a difficult task [6]. Generally, see-through HMDs have two main elements, an eyepiece, and an element guiding the image rays to the user's eye. Most of these see-through HMDs are large and heavy. In order to design a see-through HMD that is compact, the system tends to be complex and thus hard to fabricate [7]. Ways to fold the optical path are usually applied in such see-through HMD designs [7]. For example, Cheng *et al*. [8] designed a see-through HMD based on a freeform surface prism. Zheng *et al*. [9] used an x–y polynomial surface in their design for an off-axis see-through HMD. However, the aforementioned HMD systems are complex and heavy. Amitai *et al*. [10, 11] used an array of partially reflecting surfaces on a light guide substrate in their design for a see-through HMD. With this type of substrate, the light-guide elements are easier to manufacture and more compact than those for a prism-based see-through HMD. A semi-reflective coating is usually applied in the see-through HMD to extract the image rays. However, this not only increases the cost but also results in large energy loss of the virtual image because of the low transmittance. Thus, designs utilizing total internal reflection (TIR) to increase the optical efficiency of the virtual image have been developed. Hung *et al*. [12] described a light guide plate with microstructures to extract virtual image rays by TIR in their see-through HMD design which can increase the optical efficiency of the virtual image. However, the light guide plate is difficult to manufacture due to the shape of the microstructures which are inverted trapezoids relative to the light guide plate. In addition, the visibility is low with this design. In order to solve these problems, we present a new optical design for a see-through HMD.

This new design is based on a light guide plate with triangular microstructures. There are two materials in the image output region of the light guide plate. This design not only allows for extraction of the rays by TIR but also improves the manufacturability. The efficiencies of both the virtual image and real image are considered. The efficiency balance phenomenon and the suitable arrangement of the microstructures are incorporated into this design. The limitations of the optical efficiency balance performance can be overcome. In this design, the optical efficiency of the virtual image and real image are tuned by the microstructural conditions, as is the visibility. The maximum visibility obtained in previous designs was 1 [12], but the visibility range can be raised to 22 with this optical design, offering higher visibility for daily applications.

#257414 Received 28 Jan 2016; revised 18 Feb 2016; accepted 19 Feb 2016; published 25 Feb 2016

2. System specifications and optical layout for the see-through HMD

The optical see-through head mounted display based on a light guide plate with triangular microstructures is shown in Fig. 1. As can be seen in the figure, the rays from the microdisplay are incident into the light guide plate after propagating through the eyepiece. They are then reflected by a mirror and guided by TIR into the light guide plate. Finally, the rays are directed to the user's eye after striking the microstructures. The rays from the real world scene incident into the light guide plate and are extracted to the user's eye by passing through the gaps between the microstructures. The light guide plate combines the real images from the real world scene and virtual images from the microdisplay. The eyepiece collimates the rays from the microdisplay into the light guide plate and then produces a virtual image on the human eye.

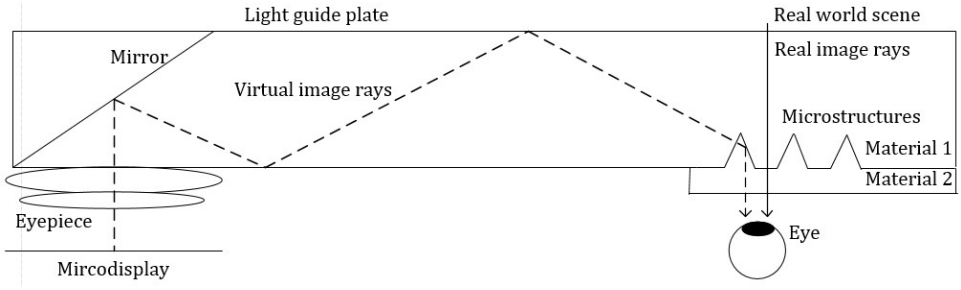

Fig. 1. Layout of the see-through HMD.

The eyepiece and the microdisplay are comprised of traditional eyepiece design with four lens elements. The microdisplay is an Organic Light Emitting Diode (OLED). With the self-emissive feature [13], the volume of the see-through HMD can be minimized. The light guide plate is used to translate the image for compact size. The specifications of the eyepiece system and OLED panel are shown in Table 1. The unfolded ray path of virtual image through the see-through HMD is shown in Fig. 2.

Table 1. Parameters and specifications of the see-through HMD system.

	Parameters	Specifications
Image source	Microdisplay	eMagin SVGA + (Rev3) OLED-XL
	Active area	12.75 mm × 9 mm
	Resolution	800 × 600 pixels
	Pixel size	15 μm/pixel
See-through HMD system	Effective focal length	30.69 mm
	Exit pupil diameter	8 mm
	F-number	3.83
	Field of view	30 degrees
	Eye clearance	15 mm
	Visibility	22

#257414 Received 28 Jan 2016; revised 18 Feb 2016; accepted 19 Feb 2016; published 25 Feb 2016

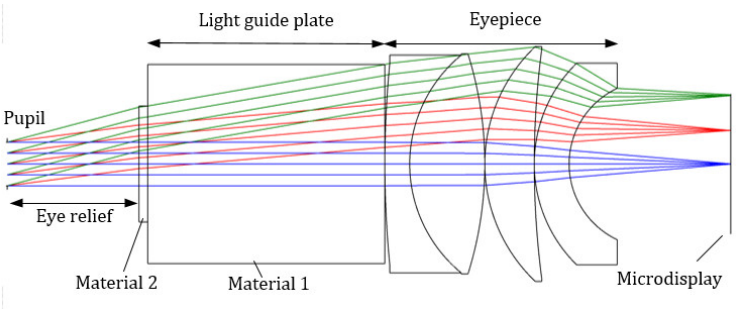

Fig. 2. Unfolded ray path of the virtual image in the see-through HMD.

In order to facilitate the discussion for the visibility in this study, the visibility is defined by taking the ratio of the optical efficiency of the virtual image E_v to the optical efficiency of the real image E_r . The visibility is also equal to the ratio of the luminance of the virtual image ($Luminance_v$) and real image ($Luminance_r$). The luminance is at the position of retina.

$$Visibility = \frac{E_v}{E_r} = \frac{Lu\min ance_v}{Lu\min ance_r}. \tag{1}$$

3. The working principles of the light guide plate with triangular microstructures

3.1 Lower limit of the angular relation

In order to ensure the appropriate propagation of rays to and extraction from the light guide plate by TIR, there are some boundary conditions that should be considered in the relationship of the angular relation between the light guide plate and the mirror [14]. As illustrated in Fig. 3, the angle between the mirror and the light guide plate is defined as φ. The refractive index of Material 1 in Fig. 1 is defined as n_1. The rays (defined as R_0) pass through the eyepiece and then propagate normally to the light guide plate. The propagation of the rays R_0 in the light guide plate by TIR should satisfy the incident angle α condition as follows:

$$\alpha \geq \sin^{-1}\frac{1}{n_1}, \tag{2}$$

$$\alpha = 2\varphi \tag{3}$$

The field of view (FOV) of the see-through HMD is further considered. The rays passing through the eyepiece and then obliquely propagating into the light guide plate are defined as R_1 and R_2. As shown in Fig. 3, the half FOV θ is the angle between the rays R_0 and the rays R_1 and R_2. The incident angle of R_1 becomes α' and the incident angle of R_2 becomes α''. The relation between the angle φ and the incident angles α' and α'' can be described as in Eq. (4). The propagation of the rays R_1 and R_2 within the light guide plate by TIR should satisfy the incident angle condition as formulated in Eq. (5). Substituting Eqs. (4) and (5), the boundary equation of the angle φ can be obtained as in Eq. (6):

$$\alpha' = 2\varphi - \theta, \alpha'' = 2\varphi + \theta; \tag{4}$$

$$\alpha' \geq \sin^{-1}\frac{1}{n_1}, \alpha'' \geq \sin^{-1}\frac{1}{n_1}; \tag{5}$$

$$\varphi \geq \frac{1}{2}\sin^{-1}\frac{1}{n_1} + \frac{\theta}{2}, \varphi \geq \frac{1}{2}\sin^{-1}\frac{1}{n_1} - \frac{\theta}{2}. \tag{6}$$

Thus, the value of the lower limit of the angle φ is selected as follows:

#257414 Received 28 Jan 2016; revised 18 Feb 2016; accepted 19 Feb 2016; published 25 Feb 2016

$$\varphi \geq \frac{1}{2}\sin^{-1}\frac{1}{n_1}+\frac{\theta}{2}. \tag{7}$$

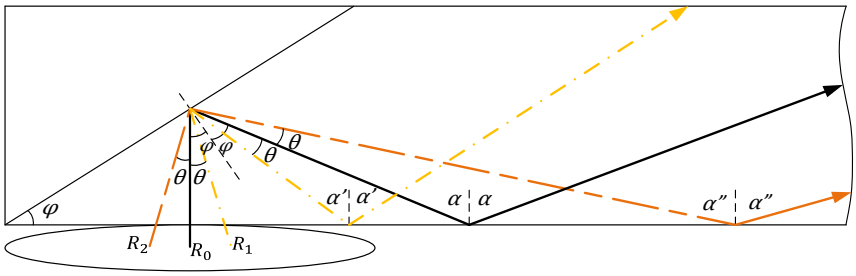

Fig. 3. Schematic diagram of the rays guided into the light guide plate: (a) The rays propagating into the light guide plate are guided by TIR.

3.2 Upper limit of the angular relation

According to Fig. 4, in order to ensure that the rays are reflected by TIR on the triangular microstructures, the refractive index of material 1(n_1) in the triangular microstructures should be lower than the refractive index of material 2(n_2), as shown in Eq. (8). Thus, when the rays R_0 strike the triangular microstructures, they are reflected by TIR. The incident angle μ should satisfy the TIR condition expressed in Eq. (9). The relations between the incident angle μ, the angle φ and the two bottom angles β and γ of the microstructure are shown in Eqs. (10), (11) and (12).

$$n_1 < n_2, \tag{8}$$

$$\mu \geq \sin^{-1}\frac{n_1}{n_2}, \tag{9}$$

$$\mu = 180° - \alpha = 90° - \varphi, \tag{10}$$

$$\gamma = \mu, \tag{11}$$

$$\beta = 2\varphi. \tag{12}$$

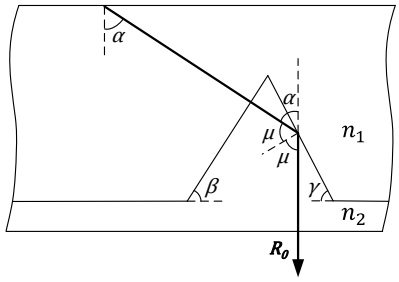

Fig. 4. Normal incident rays R_0 strike the microstructure and are reflected by TIR.

Consider the FOV of the see-through HMD, the incident angle of R_1 striking the microstructures becomes μ'. The incident angle of R_2 striking the microstructures becomes μ''. As illustrated in Figs. 5(a) and 5(b), the incident angles μ' and μ'' are described by

$$\mu' = \mu + \theta', \mu'' = \mu - \theta\ '', \tag{13}$$

while the relation between the half FOV θ and the angles θ' and θ'' is obtained from

#257414 Received 28 Jan 2016; revised 18 Feb 2016; accepted 19 Feb 2016; published 25 Feb 2016

$$\theta' = \theta\ '' = \sin^{-1}(\frac{n_1}{n_2}\sin\theta). \tag{14}$$

When the rays R_1 and R_2 strike the triangular microstructures, they are reflected by TIR where the incident angles μ' and μ'' should satisfy the following TIR conditions:

$$\mu' \geq \sin^{-1}\frac{n_1}{n_2}, \mu'' \geq \sin^{-1}\frac{n_1}{n_2}. \tag{15}$$

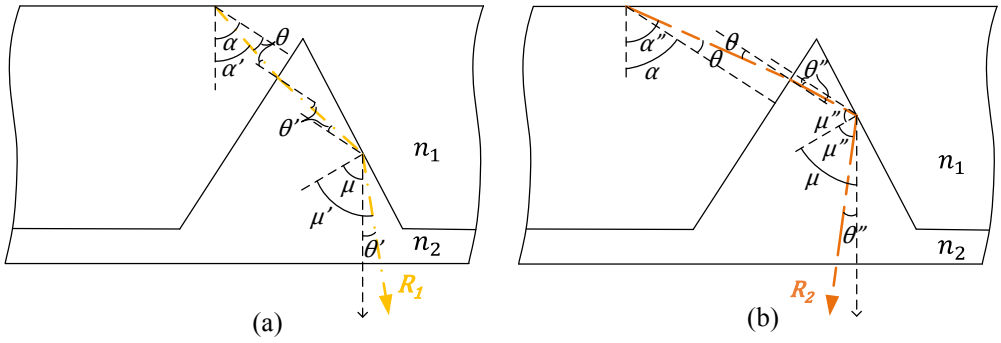

Fig. 5. (a) and (b) The oblique incident rays R_1 and R_2 strike the microstructure and are reflected by TIR.

Substituting Eqs. (13), (14) into Eq. (15), the boundary equation for the angle μ, the half FOV θ and the two refractive indices of the materials can be formulated as in Eq. (16). Then, substituting Eq. (10) into Eq. (16), the boundary equation for the angle φ, the half FOV θ and the two refractive indices of the materials can be formulated as Eq. (17).

$$\mu \geq \sin^{-1}(\frac{n_1}{n_2}) - \sin^{-1}(\frac{n_1}{n_2}\sin\theta), \mu \geq \sin^{-1}(\frac{n_1}{n_2}) + \sin^{-1}(\frac{n_1}{n_2}\sin\theta), \tag{16}$$

$$\varphi \leq 90° - \sin^{-1}(\frac{n_1}{n_2}) + \sin^{-1}(\frac{n_1}{n_2}\sin\theta), \varphi \leq 90° - \sin^{-1}(\frac{n_1}{n_2}) - \sin^{-1}(\frac{n_1}{n_2}\sin\theta), \tag{17}$$

Thus, the value of the upper limit of angle φ is selected as follows:

$$\varphi \leq 90° - \sin^{-1}(\frac{n_1}{n_2}) - \sin^{-1}(\frac{n_1}{n_2}\sin\theta). \tag{18}$$

3.3 Boundary condition and relationship of microstructure

Combining Eqs. (7) and (18), the range of the angle φ can be obtained as in Eq. (19). Further substituting Eqs. (10), (11), (12) into Eq. (19), the boundary equation for γ, β, the half FOV θ and the two refractive indices of the different materials can be derived as in Eqs. (20) and (21), respectively.

$$\frac{1}{2}\sin^{-1}\frac{1}{n_1} + \frac{\theta}{2} \leq \varphi \leq 90° - \sin^{-1}(\frac{n_1}{n_2}) - \sin^{-1}(\frac{n_1}{n_2}\sin\theta), \tag{19}$$

$$\sin^{-1}(\frac{n_1}{n_2}) + \sin^{-1}(\frac{n_1}{n_2}\sin\theta) \leq \gamma \leq 90° - \frac{1}{2}\sin^{-1}\frac{1}{n_1} - \frac{\theta}{2}, \tag{20}$$

#257414 Received 28 Jan 2016; revised 18 Feb 2016; accepted 19 Feb 2016; published 25 Feb 2016

$$\sin^{-1}(\frac{n_1}{n_2})+\theta \le \beta \le 180^\circ - 2\sin^{-1}(\frac{n_1}{n_2})+2\sin^{-1}(\frac{n_1}{n_2}\sin\theta). \quad (21)$$

Equations (19), (20) and (21) show the relation among the half FOV, two bottom angles of the microstructure, and two refractive indices of the different materials. The FOV is a significant parameter in the see-through HMD design. For most applications of a compact see-through HMD, the FOV is typically around 25 to 40 degrees [15,16]. According to Eqs. (19), (20) and (21), the FOV of the see-through HMD system is related to the refractive indices of the two materials shown in Fig. 1. The FOV is larger when the difference between the refrative indices of the two materials is larger. Thus, in this study, PMMA is used as the lower-refraction material 1 and the refractive index of material 2 is larger than 1.88 in our design. Table 2 lists several combinations with higher-refraction materials obtained from OHARA and SCHOTT. The FOVs of these combinations are also listed in Table 2.

Table 2. Relations between the combinations of two materials and the FOVs of the see-through HMDs.

Material 1	n_1	Material 2	n_2	price	FOV(2θ)
		OHARA			
PMMA	1.49	S-LAH58	1.882997	37.5	25.6
PMMA	1.49	S-NPH 2	1.922860	14.0	28.4
PMMA	1.49	S-NPH 3	1.959060	13.0	30.8
PMMA	1.49	S-LAH79	2.003300	78.0	33.6
		SCHOTT			
PMMA	1.49	N-LASF31A	1.88300	17.0	25.6
PMMA	1.49	N-LASF46A	1.90366	6	27.2
PMMA	1.49	N-SF66	1.92286	16.0	28.4
PMMA	1.49	P-SF68	2.00520	85	33.8

4. The optical efficiency for different microstructure conditions

The focus in many see-through HMD designs has only been on how to increase the optical efficiency of the virtual image. However, the optical efficiency of the real image is also important and the relation between the these two features is very important in see-through HMD applications. Some of the high refraction materials shown in Table 2 offering the large FOV in the see-through HMD can be expensive, while the the high refraction materials S-NPH2 and S-NPH3 are relatively cheaper. The high refractive index material S-NPH3 which can offer an FOV of 30.8 degrees is selected as suitable for our design. Figure 6 shows the simulation results for the combination of PMMA and S-NPH3 under different microstructure conditions. Microstructure sizes of 50μm, 40μm, 30μm, 20μm, and 10μm are simulated for analysis for the corresponding pitch. The different colors represent different sizes of microstructure. The optical efficiency is defined as a percentage of the flux of the rays extracted from the light guide plate divided by the flux of the rays entering the light guide plate. This figure shows the relation between the optical efficiency of the virtual image and the optical efficiency of the real image. The results indicate that the optical efficiency of the virtual image decreases as the pitch d increases. In contrast, the optical efficiency of the real image increases as the pitch d increases. With the same microstructure conditions, the variation of the optical efficiency of both the virtual and real image becomes larger as d gets smaller. In other words, the optical efficiency is more sensitive to the variation of the pitch as d gets smaller. Moreover, under different microstructure conditions, the variation of the

#257414 Received 28 Jan 2016; revised 18 Feb 2016; accepted 19 Feb 2016; published 25 Feb 2016

optical efficiency is larger when the size of the microstructure is smaller. In other words, the optical efficiency is more sensitive to the variation of d when the size is smaller.

The balance in optical efficiency has been found to be constant under different microstructure conditions in previous research [12]. However, with our design we can overcome the limitation of the optical efficiency balance phenomonen. Previously, the optical efficiency of the virtual image could only be increased to the same as the efficiency of the real image. This limitation was due to the design of the microstructures. Using the new microstructure design, the optical efficiency of the virtual image can be increased to be larger than the optical efficiency of the real image.

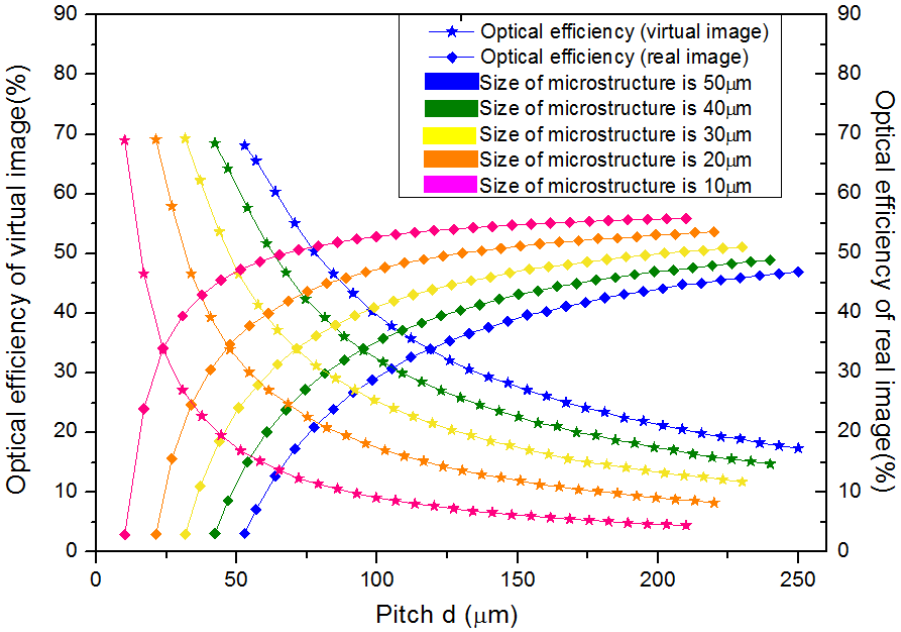

Fig. 6. Simulated values of the optical efficiencies of the virtual image and the real image under different microstructure conditions.

5. The visibility of the see-throughHMD system

Besides the optical efficiency, the visibilty of the microdisplay against the real word scene is very important for a see-through HMD display [17]. The definition of the visibility is described as Eq. (1).

As has been shown in previous research, for daily applications, the visibility is low when the optical efficiency of the virtual image is equal to the optical efficiency of the real image. The reason is that the luminance of the ambient light from the real world scene (1cd/cm^2) is always stronger than the luminance of the microdisplay (0.015cd/cm^2) [18]. Thus, for conditions under high ambient light, the optical efficiency of the virtual image should be larger than the optical efficiency of the real image. In this new design, this can be achieved, as shown in Fig. 7. The microstructure which size is 50μm is chosen as an example by typical size of brightness enhancement film. In addition, the microstructures arranged in a periodic array will generate the effect of diffraction when the size and pitch of microstructures are closer to the wavelength [19]. But the size of microstructures (50μm) is much larger than the wavelength of visible light, the diffraction effect will not almost happen. The red dashed line indicates the efficiency balance condition under which the optical efficiency of the virtual image is equal to the optical efficiency of the real image. The visibility is 1. The region to the left side of the red dashed line indicates suitable conditions for a see-through HMD. Below

#257414 Received 28 Jan 2016; revised 18 Feb 2016; accepted 19 Feb 2016; published 25 Feb 2016

this region, the optical efficiency of the virtual image is higher than the optical efficiency of the real image. The visibility will be 22 when the pitch is 53μm. The visibility obtained with the new design is much higher than the visibility obtained with the previous design making this more suitable for see-through HMDs in daily applications.

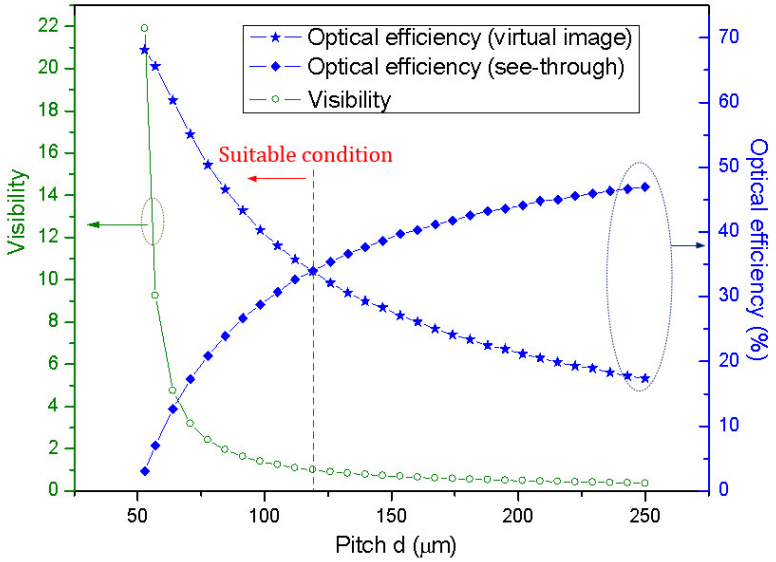

Fig. 7. Suitable conditions for a see-through HMD for daily applications and visibility of the see-through HMD with a size of 50μm.

For see-through function, the rays of real image from the real world scene are extracted to the user's eye by passing through the gaps between the microstructures strikes the microstructures as the green line illustrated in Fig. 8. However, part of the real image rays strike the microstructures and are refracted as red line and blue line illustrated in Fig. 8(a). In fact, this phenomenon maybe causes the multiple image for user when these three path-different rays all incident into the user's eye. So the position of the eye in the eyebox should be slightly modified to avoid the rays which are refracted by the microstructures incident into eye. The eyebox is the working region for the user to see the all field of the virtual image from the microdisplay. However, as illustrated in Fig. 8(b) and 8(c), there are still rays which are refracted by the microstructures incident into eye when the incident angle of ambient rays larger than 10 degrees.

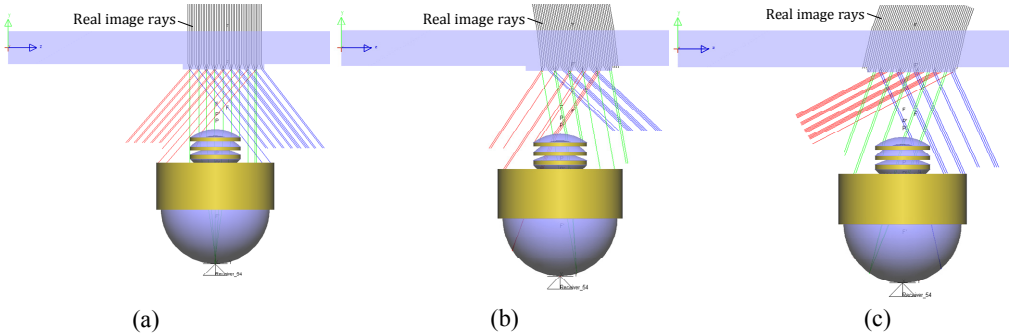

Fig. 8. Multiple image for the see-through HMD. (a) normal incident rays of the real image, (b)and(c) oblique incident rays of the real image.

#257414 Received 28 Jan 2016; revised 18 Feb 2016; accepted 19 Feb 2016; published 25 Feb 2016

6. System layout and tolerance analysis

According to above discussion, the parameters of the see-through HMD system for our design are φ = 29.1°, β = 58.2°, γ = 60.9°, the size of the microstructure is 50μm and the pitch d is 53μm. The whole system model is simulated in LightTools software, as shown in Fig. 9.

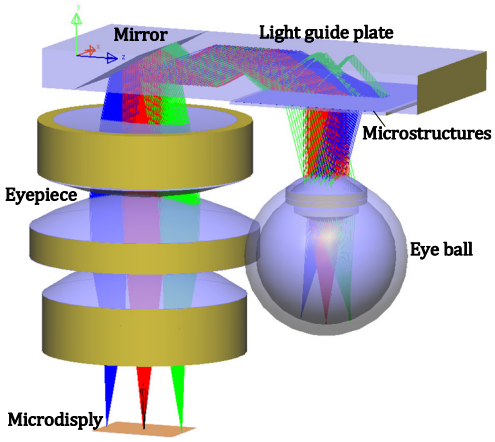

Fig. 9. The layout of the see-through HMD and eye model demonstrated with LightTools.

Among the working principles for microstructures, the angle of the microstructure is an important parameter for tolerance analysis. The tolerance of the microstructure to be used in a see-through HMD under different FOVs given the two bottom angles γ and β is evaluated. The results showing the dependence of the bottom angles γ and β and the FOV are shown in Fig. 10. As can be seen from this figure, the tolerance level of the two bottom angles γ and β increases with decreasing FOV. In our design, the FOV of the see-through HMD is 30°, and the tolerance level of the two bottom angles γ and β are 0.55° and 1.11°, respectively. For the manufacturing process, we will try to use the previous manufacture process for lens array [20]. In this manufacture process, we must use the ultra-high precision tooling machine to produce the master mold. For the ultra-high precision tooling, the angle tolerance is very small. Under the demold process, the angle tolerance can be controlled under 0.25 degree. The tolerance degree is like the commercial optical fabrication level [21], so the tolerance level for manufacturing is acceptable.

#257414 Received 28 Jan 2016; revised 18 Feb 2016; accepted 19 Feb 2016; published 25 Feb 2016

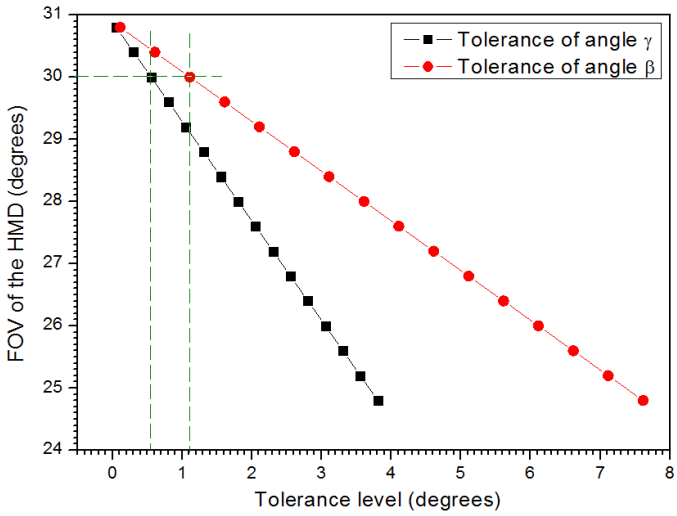

Fig. 10. Tolerance level of the two bottom angles γ and β of the microstructure and the FOV of the see-through HMD.

Figure 11 shows a schematic representation of the microstructures with different error angles θ_e. Error angles from −1 to 1 degree were simulated using the optical simulation software. The dependence of the optical efficiency of the virtual image and the real image on the error angle θ_e is illustrated as Fig. 11. We found that the influence of the error angle of the microstructure on the optical efficiency of the real image is very small, because the microstructure is used to extract light for the virtual image. The error angle θ_e did not change the gap between the microstructures which allowed the ambient light to pass through so did not influence the optical efficiency of the real image. However, θ_e did influence the optical efficiency of the virtual image. This was due to the light from the microdisplay striking the microstructures and then being extracted by TIR. When there was no error angle θ_e, the optical efficiency of the virtual image reached its maximum. When there was error angle θ_e, the TIR conditions were destroyed, and the optical efficiency decreased. The data in Fig. 12 indicate a decrease in the optical efficiency of the virtual image of 0.13% for an error angle θ_e of −1°, and a decrease of 1.07% when the error angle θ_e is 1°. In general, an error angle not greater than 0.25° is acceptable for commercial optical fabrication [20,21].

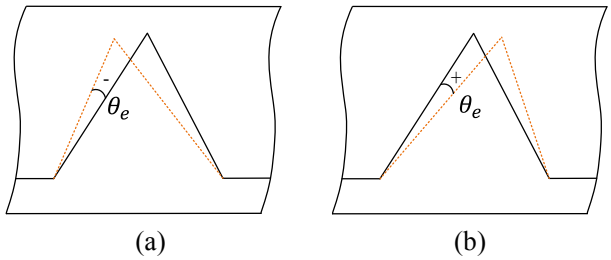

Fig. 11. Microstructure with error angles θ_e of (a) −1°; (b) 1°.

#257414 Received 28 Jan 2016; revised 18 Feb 2016; accepted 19 Feb 2016; published 25 Feb 2016

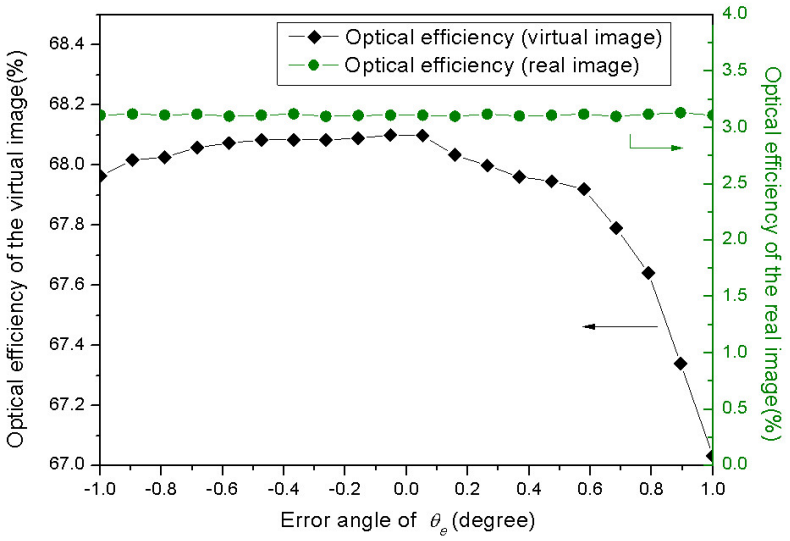

Fig. 12. Dependence of the optical efficiency of the virtual and the real image on the error angle θ_e.

7. Conclusion

An optical design for a see-through HMD with high visibility is presented. This design is based on a light guide plate with triangular-shaped microstructures. The working principles of the system are described in detail. For the manufacturing process, we will try to use the lens array manufacture process for triangular-shaped microstructures [20]. In this manufacture process, there are three main steps for production. The first step is dispensing. The second step is embossing and curing. The third step is demolding. In comparison to the inverted trapezoidal shape of the microstructures in previous designs [12], the triangular-shaped microstructures in our new design are easier to manufacture. Moreover, the limitations to the optical efficiency balance phenomenon discussed in previous studies can be overcome. In addition, the concept of visibility is taken into account in this design. For practical HMD applications the visibility should be at least larger than 1. In other words, the optical efficiency of the virtual image should be larger the optical efficiency of the real image. The maximum visibility obtained with previous designs was 1 due to the limited balance in optical efficiency. With this novel design, however, the visibility can be increased to 22, much higher than for previous designs, making this system more suitable for use in see-through HMDs for daily applications.

Acknowledgments

This study was supported in part by the Ministry of Science and Technology, Taiwan, project number MOST104-2220-E-009-006 and MOST104-2622-E-009-012-CC3.

#257414 Received 28 Jan 2016; revised 18 Feb 2016; accepted 19 Feb 2016; published 25 Feb 2016